PA6/Clay Nanocomposites by Continuous Sonication Process

Sarat K. Swain,* Avraam I. Isayev

Institute of Polymer Engineering, The University of Akron, Akron, Ohio 44325-0301

Received 21 October 2008; accepted 15 March 2009
DOI 10.1002/app.30827
Published online 7 July 2009 in Wiley InterScience (www.interscience.wiley.com).

ABSTRACT: Polyamide 6 (PA6)/clay nanocomposites were prepared using a single screw extruder with an ultrasonic die attachment. The die pressure and ultrasonic power consumption were measured at various clay concentrations. The structure and morphology of nanocomposites studied by X-ray diffraction (XRD) and transmission electron microscopy (TEM) indicated that the clay (Cloisite® 30B) was exfoliated within PA6 matrix at all clay concentrations, while clays (Cloisite® 15A and 93A) only intercalated. The complex viscosities of the nanocomposites were increased with clay loading and after ultrasonic treatment at lower amplitudes. The Young's modulus, stress and elongation at break, toughness and yield stress and strain of ultrasonically treated nanocomposites were significantly affected by the level of intensity of ultrasound. In addition to XRD, differential scanning calorimetry (DSC) and ^{15}N NMR techniques were used to investigate the structural changes in PA6/clay nanocomposites. The results indicated that the intercalated organoclay nanocomposites can induce generation of the γ-form crystal of PA6 and substantially affect the arrangement of molecules in the α-form crystal. It was found that the addition of clay in the PA6 matrix leads to a decrease of crystallinity. However, ultrasonic treatment of nanocomposites increased crystallinity. A substantial reduction in oxygen permeability was observed by increasing concentration of clay. © 2009 Wiley Periodicals, Inc. J Appl Polym Sci 114: 2378–2387, 2009

Key words: clay; nanocomposites; polyamides; processing; structure

INTRODUCTION

Polymer-based composites have received high interest due to their unusual combination of stiffness and toughness that are difficult to attain from individual components. For this reason, they have been widely used in areas of transportation, construction, electronics, and consumer products. Nanocomposites exhibiting a change in composition and structure over a nanometer length scale have been shown over the last few years to afford remarkable property enhancements relative to conventional composites.[1–3] Organically modified clays can be effective reinforcing agents in manufactured polymer-clay nanocomposites. By inserting long-chain surfactants into the hydrophilic galleries of the native clay, the interlayer distance increases, and the surface chemistry of the clay is modified.[4] Two terms, intercalated and exfoliated, are used to describe the two general classes of nanomorphology that can be prepared.[5] Intercalated structures are well-ordered multilayered structures where the extended polymer chains are inserted into the gallery space between the individual silicates layers. The exfoliated structures result when the individual silicate layers are no longer close enough to interact with the adjacent layers gallery cations. The coupling between the tremendous surface area of the clay and the polymer matrix facilitates stress transfer to the reinforcement phase, allowing for strength and toughness improvements. Conventional polymer-clay composites containing aggregated fillers ordinarily improve rigidity, but they often sacrifice strength, elongation, and toughness.[6] However, exfoliated clay nanocomposites show improvement in all aspects of their mechanical, rheological, and thermal properties. Polymer-clay nanocomposites have unique properties when compared with conventional filled polymers.[7–11] For example, the mechanical properties of a Nylon 6 layered-silicate nanocomposite, with a silicate mass fraction of only 5%, show excellent improvement over those for the pure Nylon 6.[7] The nanocomposite exhibited a higher tensile and flexural strength, Young's and flexural modulus with the impact strength being lowered by only 10%.[12]

Nylon 6 is a polymer material with low cost and high performance, which has found wide applications in the field of fibers, films, and other engineering products. There are two crystalline forms in

**Present address:* Department of Chemistry, North Orissa University, Takatpur, Baripada-757003, India
Correspondence to: A. I. Isayev (aisayev@uakron.edu).
Contract grant sponsor: NSF; contract grant number: CMMI-0654326.

Nylon, α-, and γ-form.[13–16] The thermodynamically stable crystalline α-form consists of fully extended planar zigzag chains, in which adjacent antiparallel chains are joined by the hydrogen bonds. It can be obtained by slowly cooling from the melt. The less stable γ-phase is composed of pleated sheets of parallel chains joined by the hydrogen bond. It can be obtained by fiber spinning at a high speed or by fast cooling from the melt.[17,18] The γ-form can be converted into α-form by melting followed by recrystallization, by annealing at 160°C in a steam-saturated atmosphere without any significant loss of orientation or by applying stress at room temperature.[19,20] Extensive studies of polyamide-based clay nanocomposites by incorporating organically modified clays were first conducted on Nylon 6 by the Toyota research group.[21,22]

Several studies on the application of ultrasound in nanocomposites preparation were reported using static[23,24] and continuous[25–28] processes. It should be noted that in the static process an ultrasonic horn is typically placed in a stationary cup containing nanocomposite, whereas in the continuous process an ultrasonic horn is placed in the extrusion die or barrel. The most recent attempts to develop polymer/clay nanocomposites via melt intercalation in batch mixers with power ultrasound were reported.[29–31] However, prolonged ultrasonic treatment (10–20 min) was used in these studies, apparently leading to a substantial degradation of the polymer matrix. Despite the considerable number of studies concerned with the preparation, characterization, and properties of PA6/clay nanocomposites, no report has been published regarding their processing by ultrasonic-assisted extrusion process.

Over the past several decades, a number of studies of the effects of ultrasound on the extrusion of polymers have been performed.[25–28,32,33] It was observed that long-chain polymer molecules can be ruptured by high-intensity ultrasound during melt extrusion leading to the formation of long-chain radicals.[25] In polymer-clay systems, polymeric radicals may combine with the surface modifying agent of the clay forming chemical bonds. Another important aspect of the ultrasound assisted process was to facilitate the break up and delamination of layered silicate, which is essential for the nanoscale dispersion of clays during melt mixing with the polymer matrix in the extruder.[32,33]

In this article, PA6/clay nanocomposites were prepared using a single screw extrusion process without and with imposition of ultrasonic waves. The combined effects of clay dispersion and continuous ultrasonic treatment during melt extrusion of PA6/clay nanocomposites on their structural, mechanical, rheological, crystallization, and gas permeation properties are reported. An order magnitude reduction in oxygen permeability is reported with an increase of clay concentration.

EXPERIMENTAL

Materials and methods

The polyamide 6 (PA 6) used was Ultramid B40LN (BASF). Before processing, it was dried at 80°C for 24 h. Cloisite® 15A, 93A, and 30B are natural montomorillonite, organically modified with quaternary ammonium salts, were supplied by Southern Clay Products (Austin, TX).

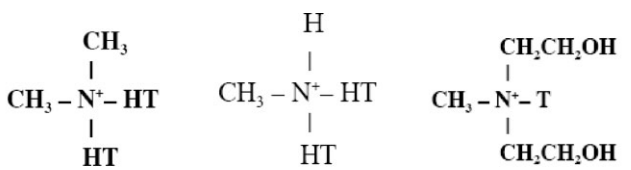

Cloisite® 15A Cloisite® 93A Cloisite® 30B

where T is tallow (~65% C18; ~30% C16; ~5% C14).

PA6/clay nanocomposites of clay contents of 2.5, 5.0, and 10.0 wt % were prepared by single screw compounding extruder with the ultrasonic slit die attachment.[33] Two horns were inserted into a slit die having a gap size of 4 mm. These horns supplied ultrasonic waves at a frequency of 20 kHz and amplitudes of 5, 7.5, and 10 μm. The screw was equipped with two mixing sections (Maddock mixer followed by melt-star mixer). A screw speed of 100 rpm and temperatures of 220, 225, and 230°C from the feeding section to the die zones, respectively, were utilized. The material was ultrasonically treated in the molten state at a flow rate of 0.50 g/s corresponding to a residence time of 14 s. The details of the ultrasonic extruder were published elsewhere.[33]

Measurement of properties

Tensile bars were prepared by a Van Dorn 55 HPS 2.8F injection molding machine at a melt temperature of 230°C, injection speed of 76.2 mm/s, holding pressure of 17.2 MPa, holding time of 20 s, and cooling time of 40 s. The tensile stress–strain behaviors of nanocomposites were measured according to ASTM D-638-00 using an Instron testing machine Model 5567. Tests were carried out at a crosshead speed of 50 mm/min and 30 KN load cell without the use of an extensiometer. The five specimens for each composition were used for measurement and average values were reported.

The rheological properties were measured by ARES, TA Instruments, in dynamic mode of frequency sweep (strain control) process at 230°C. Parallel plate geometry with a diameter of 25 mm and a gap size of 1.9 mm was used. Samples for ARES

were prepared by compression molding for 10 min at a pressure of 20.5 MPa using a compression molding press (Carver 4122, Wabash, IN). A mold with four identical cavities was placed between the plates at 240°C, and the polymer pellets were spread out in the cavities with a diameter of 25 mm and a depth of 2 mm. The plates were closed but not tightened and kept at that level for 5 min to allow the pellets to melt. After melting, the plates were closed with slight pressure and opened periodically to remove the bubbles inside. The pumping procedure took another 5 min. The plates were then closed and kept at a pressure of 20.5 MPa for another 5 min.

The thermal behavior of the nanocomposites was measured by Differential Scanning Calorimeter (DSC, TA Instruments V3.0G, Wilmington, DE). Samples were heated from room temperature to 250°C at a rate of 10°C/min under nitrogen atmosphere.

X-ray diffraction (XRD) patterns were obtained using a Rigaku X-ray machine operating at 40 kV and 150 mA. This allowed us to determine the mean interlayer spacing of the (001) plane (d_{001}) for the organoclays and its PA6 nanocomposites.

A transmission electron microscope (TEM, TECNAI 12, Philips) operating at 120 kV was used to study the morphology of nanocomposites. A Reichert Ultracut low-temperature sectioning system equipped with diamond knife was used to cut ultrathin specimens of 75 nm by cryoultramicrotome below the glass transition temperature of PA6 to maintain the rigidity of the specimen. The specimens were transferred into a copper grid.

Solid-state ^{15}N NMR spectra were obtained at 4.7 T using a Varian Inova 200 MHz (^{1}H frequency) spectrometer with a Doty Scientific supersonic MAS probe. All ^{15}N spectra were acquired using a ramped cross polarization[34] with a magic angle spinning (MAS) speed of 3 kHz, 2 s relaxation delay, 1 ms contact time, 7.5 μs 90° pulse width, and a 50 kHz decoupling field. Each experiment required ~9.5 h to acquire 16,384 transients. Samples were packed into 7 mm silicon nitride rotors with kel-f end caps. ^{15}N chemical shifts were corrected by using ammonium nitrate ($\delta_{NH4} = 0$ ppm) as an external reference.

Oxygen permeability of the films was measured using an oxygen permeation analyzer (Illinois Instrument, Model 8001, Johnsburg, IL). Films of 0.5 mm thickness were prepared by compression molding at a pressure of 27.5 MPa and temperature of 230°C. To prevent the materials from sticking to the molding plates, Teflon foil was used. All sample films were cut into a circular shape of 10 cm diameter. Measurements were carried out in presence of nitrogen gas with a purge rate of 1 unit. Oxygen permeability of nanocomposites in units of cm^3 $mm/m^2/24$ h was measured.

RESULTS AND DISCUSSION

PA6/clay nanocomposites of Cloisite® 15A, 93A, and 30B clays at concentration of 5 wt % were prepared. It was found that Cloisite® 30B is highly dispersed in PA6 when compared with Cloisite® 15A and 93A. X-ray diffraction of each clay and there respective nanocomposites were compared. As discussed later (Fig. 2), the XRD peaks of Cloisite® 15A and 93A appeared at lower 2θ values, whereas that peak was disappeared in case of Cloisite® 30B. It indicates nanocomposites were intercalated with Cloisite® 15A and 93A, whereas exfoliated with Cloisite® 30B.[5] Cloisite® 15A is hydrophobic in nature and hence not compatible with PA6, whereas the modified surfaces of Cloisites® 93A have a long chain in the backbone to interact with PA6. However, the hydroxyl group at the backbone of Cloisite® 30B involves an H-bond with the amine group of the polyamide to form exfoliated structures. Therefore, out of three types of clays, Cloisites® 30B is discussed in further detail.

Process characteristics

The die pressure and power consumption as a function of ultrasonic amplitude are presented in Figure 1(a,b), respectively. It was observed that the die pressure decreased tremendously with increased ultrasonic amplitude. This may be due to reduced friction between the PA6/clay composites and the die walls due to ultrasonic vibration.[35] Furthermore, it was observed that the die pressure of the neat PA6 is higher than that of the PA6/clay nanocomposites at an amplitude of 5 μm. However, the die pressure is lower for higher amplitudes of 7.5 and 10 μm. The change may be due to a permanent change in melt viscosity caused by a possible degradation of polymer chains and a temporary change of viscosity caused by thixotropic effect. Both of these effects are evidently enhanced by the presence of clay causing enhanced cavitation at lower intensity of ultrasound at an amplitude of 5 μm. The more change of viscosity occurred due to the treatment of clay nanocomposites at higher intensity of ultrasound. It was also observed that in the absence of ultrasonic treatment, the die pressure of nanocomposites decreased slightly with increase in clay loading.

The ultrasonic power consumption is due to the dissipation of energy transferred to heat, energy to disperse clay and promotion of polymer interaction with clay gallery. From Figure 1(b), the ultrasonic power consumption increases with increased ultrasonic amplitude with the curve of pure PA6 having greatest slope. It was also found that power consumption increased with increased clay loading,

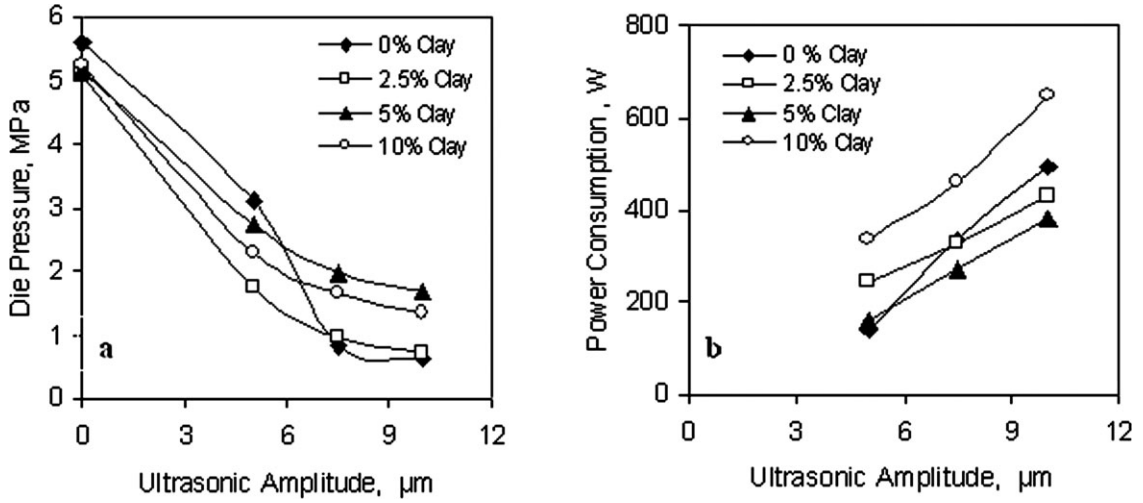

Figure 1 Die pressure (a) and power consumption (b) as a function of ultrasonic amplitude for clay (Cloisite 30B) at different concentrations.

indicating that more energy was transmitted into the system.

Structural properties

The XRD patterns of pristine clay and PA6/clay nanocomposites are summarized in Figures 2–5. It was found that in PA6/clay (30B) nanocomposites, the peak corresponding to clay 30B disappears (Fig. 2). This indicates that the fully exfoliated structure was obtained. However, PA6/clay (15A) and PA6/clay (93A) nanocomposites had XRD peaks but at lower 2θ angles than those of respective pristine clays, indicating intercalated structures with less dispersion than in the case of clay 30B.[5] The interlayer distances for different clays, Cloisites® 15A, 93A, and 30B, along with corresponding PA6/clay

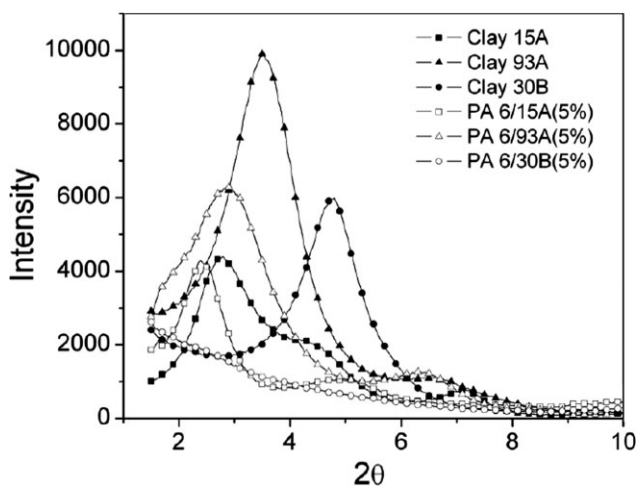

Figure 2 XRD patterns of clays 15A, 93A, and 30B and PA6/clay nanocomposites at a concentration of 5 wt % obtained without ultrasonic treatment.

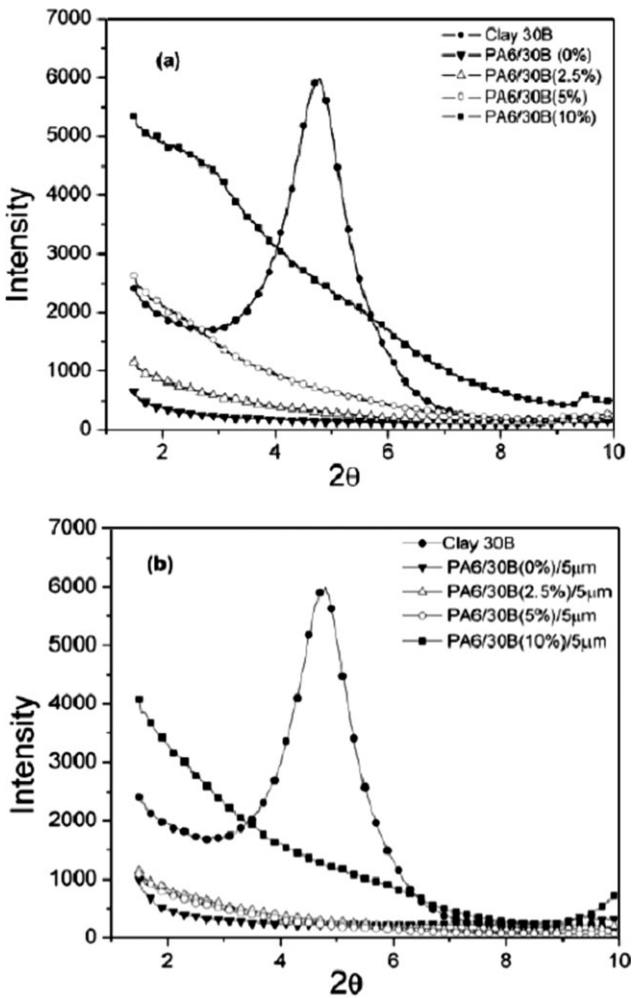

Figure 3 XRD patterns of clay (30B), PA6, and PA6/clay nanocomposites of different clay concentrations obtained without sonication (a) and with sonication at an amplitude of 5 μm (b).

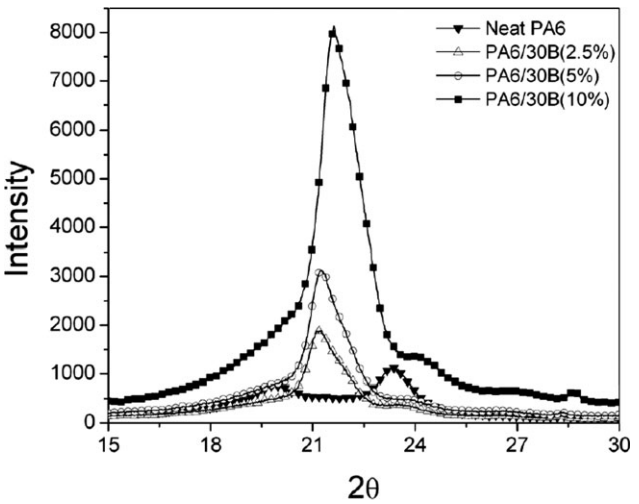

Figure 4 XRD patterns of PA6 and PA6/clay (Cloisite 30B) nanocomposites of different concentrations obtained without ultrasonic treatment.

nanocomposites were calculated by Brag's law ($n\lambda = 2d \sin\theta$). Values of the 2θ angles corresponding to the XRD peaks and corresponding interlayer spacings are shown in Table I. It is seen that there is a significant increase of the interlayer spacing in PA6/clay (15A) and PA6/clay (93A) nanocomposites in comparison with those of pristine clays. Since the fully exfoliated structure was obtained on PA6/clay (30B) nanocomposites, these nanocomposites were taken for further detailed study.

The XRD patterns of Clay 30B, PA6, and PA6/clay (30B) nanocomposites in the range of 2θ varying from 1.5 to 10° are shown in Figure 3 at various clay concentrations without sonication (a) and with sonication at an amplitude of 5 μm (b). It is observed that at all clay loadings, with or without sonication, the crystalline peaks of clay (30B) disappear indicating completely exfoliated structure of nanocomposites. It may be due to the strong interaction of amide of PA6 with functional tallow of Cloisite® 30B. Also, some changes in the XRD intensity can be observed in sonicated nanocomposites. In particular, the shoulders in the XRD intensity at an angle of 2θ of about 2.5° at concentrations of 5 and 10 wt %. that is seen in nanocomposites without sonication [Fig. 3(a)], completely disappears in the respective sonicated nanocomposites [Fig. 3(b)]. Furthermore, a reduction of the XRD intensity with sonication is evident.

Figure 4 shows that the wide angle X-ray diffraction patterns obtained at 2θ angle varying from 15 to 30° for the PA 6 sample as received and PA6/clay nanocomposites at clay concentrations of 2.5, 5, and 10 wt %. It is seen that the XRD pattern of neat PA6 shows two reflections at 2θ values of 20.5 and 23.5° indicating the presence of the α-crystalline phase, whereas PA6/clay nanocomposites show strong reflections at 2θ value of 21.5° characteristic of the γ-crystalline form of PA6.[18] These observations conclude that the α-crystalline form of PA6 was converted into the γ-crystalline form due to compounding with clay. In other words, the more stable α-form can be easily converted into less thermodynamically stable γ-form by dispersion of clay. Figure 4 also shows that intensity of the peaks was increased with increased clay loading.

Figure 5 shows the XRD patterns of PA6 as received, PA6 and PA6/clay 30B passed through extruder without and with ultrasonic treatment at loading of 2.5 wt %. From Figure 5, it was found that the PA6 as received and PA6 extruded without and with ultrasonic treatment show two peaks at 2θ values of 20.5 and 23.5° corresponding to the α-crystal form. Whereas one peak at 2θ value of 21.5° for the γ-crystal form was observed for PA6/clay nanocomposites. The probable explanation for this change in crystal form of PA6 with compounding of clay may be due to one of the following two possibilities: (i) the clay surface induces kinetically favored formation of the γ-crystal form; (ii) the clay

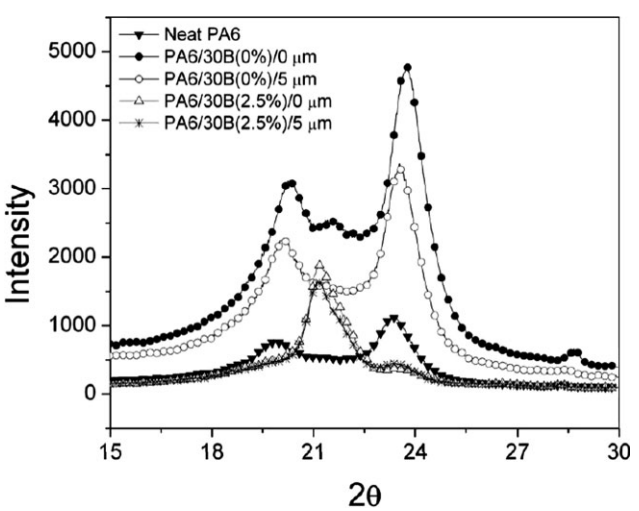

Figure 5 XRD patterns of PA6 and PA6/clay (Cloisite 30B) nanocomposites at a concentration of 2.5 wt %. obtained without and with ultrasonic treatment.

TABLE I
Comparison of d-Spacing of Various Clays and PA6/Clay Nanocomposites

Sample	2θ (°)	d-Spacing (nm)
Cloisite® 15A	2.81	3.16
PA6/15A (5%)/0 μm	2.42	3.65
Cloisite® 93A	3.48	2.36
PA6/93B (5%)/0 μm	2.94	2.97
Cloisite® 30B	4.80	1.84
PA6/30B (5%)/0 μm	No clay peak	
PA6/30B (5%)/5 μm	No clay peak	

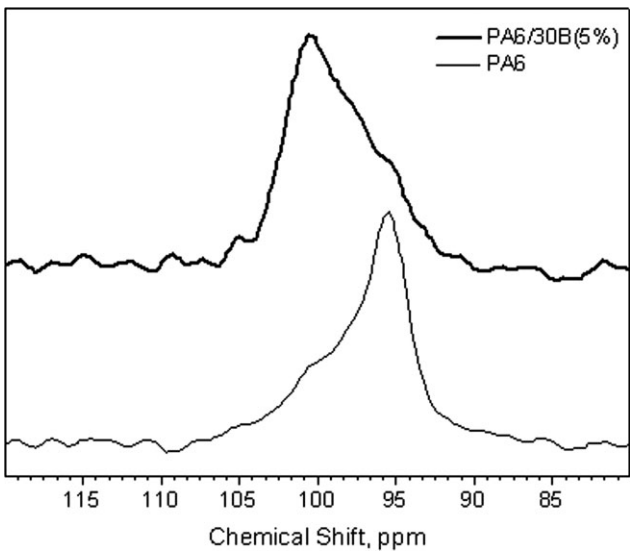

Figure 6 ^{15}N NMR of PA6 and PA6/clay (Cloisite 30B) 5 wt % without ultrasonic treatment.

changes the thermodynamics of the system such that the α-crystal form becomes less stable even at nanometer distance at clay surface. Since the latter possibility is unlikely, it is believed that the amine end groups are tightly bound to the clay surface, but not arrayed on the surface at an interchain distance. This allows the formation of the layered hydrogen bonded sheets of the γ-crystal form.

The observed changes in the crystal forms of PA6 were further supported by ^{15}N NMR spectra of PA6 and PA6/clay composites, as indicated by Figure 6. It was found that PA6 shows a distinct peak at 95 ppm, whereas PA6/clay nanocomposites show a strong peak at 101 ppm indicating the change in crystal form due to clay loading. Since only the α-phase was observed in the neat Nylon 6 as received, the presence of the γ-phase in the composites must result from interaction with clay. On the basis of the obtained results, it can be concluded that all of the Nylon amine end groups are protonated and bound to the clay surface. Thus, in ^{15}N NMR spectra (Fig. 6), the chemical shifts of Nylon 6/clay was different from the natural amine end groups normally observed in Nylon 6.

The results concerning dispersion of clay obtained from the XRD studies were further supported by the TEM micrographs of PA6/clay 30B at loading of 5 wt % for samples obtained without and with ultrasonic treatment at an amplitude 5 μm (Fig. 7). The layered structure of untreated 5 wt % clay (Cloisite 30B) samples [Fig. 7(a)] was disrupted by ultrasonic treatment of an amplitude of 5 μm [Fig. 7(b)]. This indicates that the polymer has entered into the intergallery spacing where individual clay layers were being dispersed in the polymer matrix. This may be due to complete exfoliation that occurred under ultrasonic treatment.

Mechanical properties

The mechanical properties, including the Young's modulus (a), elongation at break (b), stress at break (c), toughness (d), yield stress (e), and yield strain (f) of PA6/clay 30B nanocomposites obtained at various ultrasonic amplitudes are plotted in Figure 8 as a function of clay loading. The Young's modulus of nanocomposites [Fig. 8(a)] increased significantly with increasing clay loading at all intensities of ultrasound. Furthermore, the Young's modulus is decreased with treatment at high ultrasonic amplitudes (7.5 and 10 μm). It is also observed that the elongation at break of nanocomposites [Fig. 8(b)] decreased with increasing clay content. Also, the elongation at break of PA6 and nanocomposites increased at an amplitude of 5 μm and reduced at an ultrasonic amplitude of 10 μm. The stress at break of both untreated and ultrasonically treated

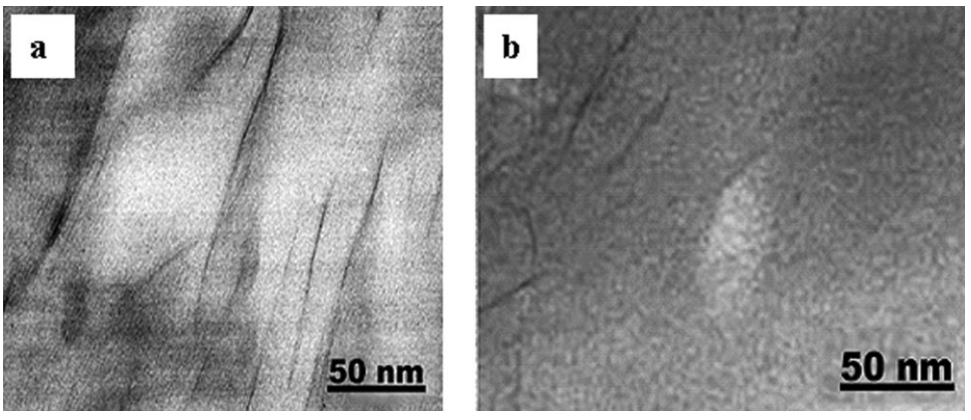

Figure 7 TEM micrographs of PA6/clay (Cloisite 30B) 5 wt % nanocomposites obtained without (a) and with (b) ultrasonic treatment at an amplitude of 5 μm.

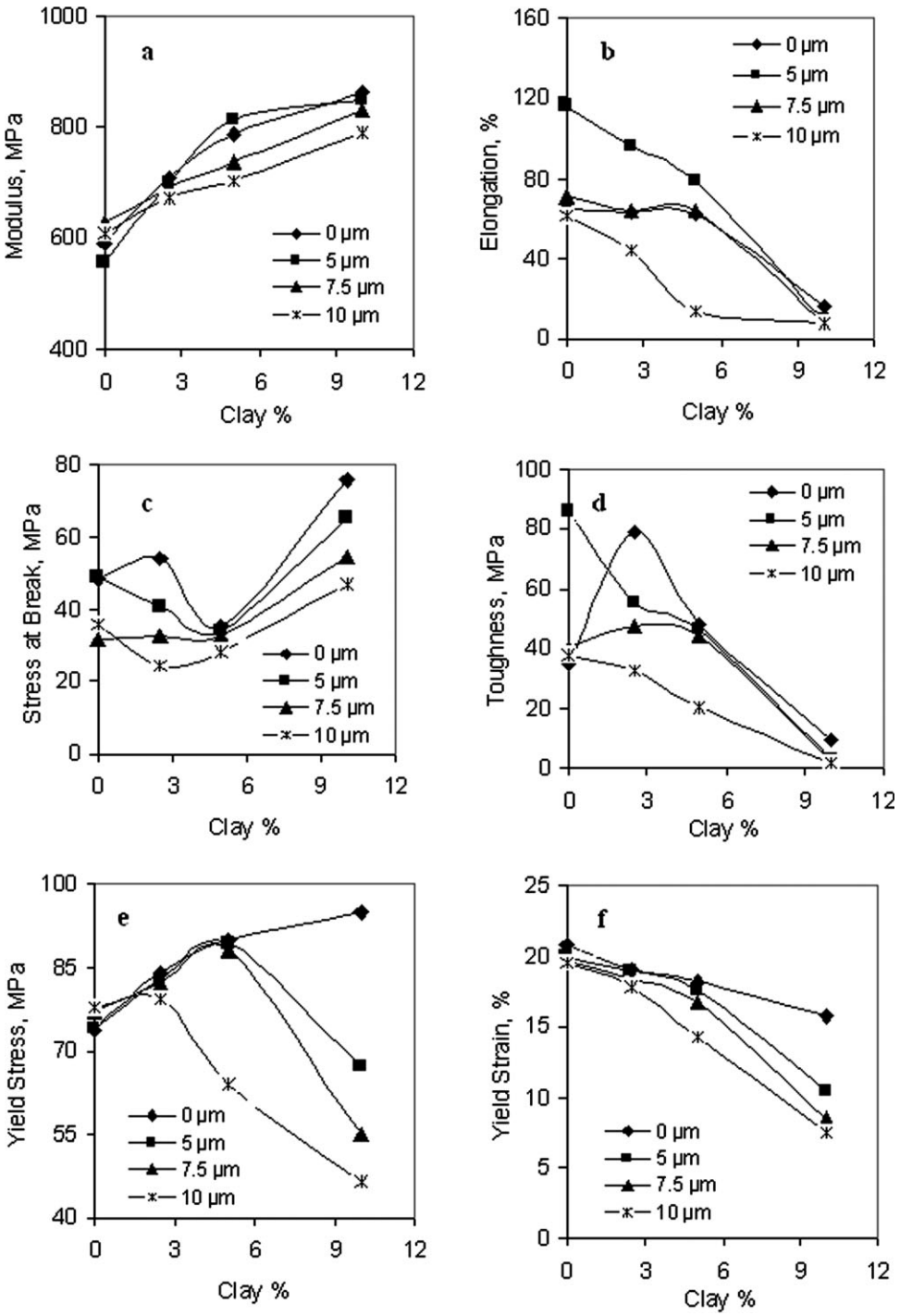

Figure 8 Young's modulus (a), elongation at break (b), stress at break (c), toughness (d), yield stress (e), and yield strain (f) as a function of clay (Cloisite 30B) concentration at different ultrasonic amplitudes.

nanocomposites [Fig. 8(c)] were decreased slightly with increase of clay concentration at 2.5 and 5 wt % and then increased tremendously at 10 wt % clay concentration. Except for PA6, the toughness of nanocomposites [Fig. 8(d)] was generally decreased with clay loading and with ultrasonic amplitude. Toughness of pure PA6 increases significantly at an ultrasonic amplitude of 5 µm. At ultrasonic amplitudes of 5 and 7.5 µm, the yield stress of nanocomposites [Fig. 8(e)] was increased with increase of clay concentration up to 5 wt %. Then, it decreased significantly at 10 wt % clay concentration. It was also found that the yield strain of nanocomposites [Fig. 8(f)] was decreased with increased clay loading at all ultrasonic amplitudes. From obtained results, it was observed that some mechanical properties were

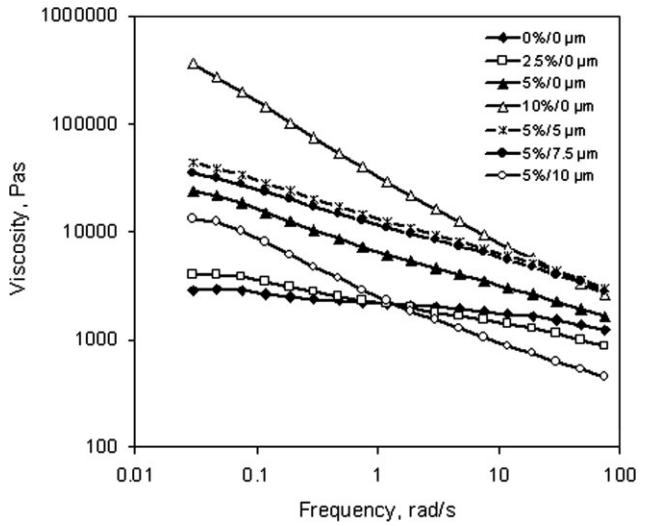

Figure 9 Complex viscosity of PA6 and PA6/clay (Cloisite 30B) nanocomposites as a function of frequency at different concentrations and various ultrasonic amplitudes at a concentration of 5 wt %.

decreased with increased ultrasonic treatment and found to be substantially lower at an ultrasonic amplitude of 10 μm. Therefore, it was concluded that both clay and ultrasonic intensity played a vital role in the dispersion of clay in the polymer matrix.[36]

Rheology and crystallization

The complex viscosity of nanocomposites as a function of frequency at various clay contents and at different ultrasonic amplitudes at 5 wt % clay concentration is illustrated in Figure 9. It is observed that the complex viscosity of untreated composites increased with increasing clay concentration. Furthermore, the complex viscosity of ultrasonically treated composites containing 5 wt % clay generally increased at ultrasonic amplitudes of 5 and 7.5 μm in comparison with the untreated sample. However, at ultrasonic amplitude of 10 μm, the complex viscosity decreased. Similar trends have been obtained at all concentrations of clay. The observed increase of the complex viscosity of nanocomposites with ultrasonic treatment was attributed to the nanoscale dispersion of the clay within PA6, which improved the compatibility between the polymer matrix and layered silicates. As a consequence of the improved compatibility of PA6/clay 30B nanocomposites, their viscosity increased and the mobility of the polymer chains was reduced which is similar as reported earlier.[27] The complex viscosity of nanocomposites was decreased with ultrasonic treatment at higher amplitude (10 μm) possibly due to degradation of polymeric chains under action of ultrasound of high intensity. However, the aforementioned restricted mobility of the polymer chains in PA6/clay nanocomposites may lead to a decrease of their crystallinity. The crystallinity of PA6 and nanocomposites at a clay loading of 5 wt % without and with ultrasonic treatment was determined from the DSC data. The results are illustrated in Table II. The degree of crystallinity (X) was determined by the equation: $X(\%) = \Delta H_f/(1-f)\Delta H_m \times 100$, where ΔH_f is the heat of fusion, ΔH_m is the extrapolated value of the enthalpy corresponding to the melting of a 100% crystalline PA6 sample and f is the weight fraction of clay in the composites. The value of ΔH_m was taken as 190 J/g.[37] It is seen that the PA6 sample exhibited an overalls higher crystallinity than the PA 6/clay nanocomposites. Similar results have also been reported earlier[38,39] where crystallinity of PA6 and PA6/clay has been calculated under different cooling conditions. Furthermore, it was observed that crystallinity of ultrasonically treated nanocomposite is higher than that of untreated sample.

TABLE II
Crystallinity of PA6 and PA6/Clay 30B Nanocomposites Without and with Ultrasonic Treatment

Sample (PA/Clay% /Amplitude)	T_m (°C)	H_m (J/g)	X (%)
PA6/0% Clay/0 μm	222.4	75.6	39.8
PA6/0% Clay/5.0 μm	220.7	65.1	34.3
PA6/5% Clay/0 μm	220.0	38.5	21.4
PA6/5% Clay/5.0 μm	220.9	45.7	25.3

Oxygen permeability

Polymer-layered silicate nanocomposites, which have shown to inhibit oxygen permeation, are being

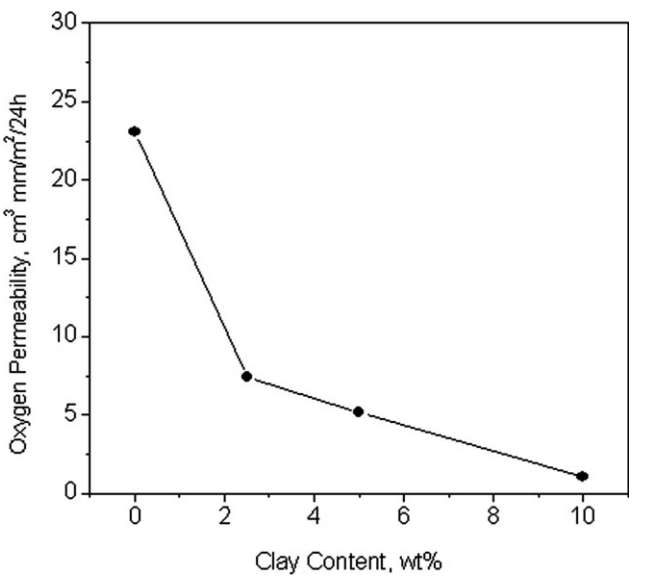

Figure 10 Oxygen permeability as a function of clay concentration for PA6 and PA6/clay (Cloisite 30B) nanocomposites obtained without ultrasonic treatment.

TABLE III
Oxygen Permeability of PA6 and PA6/Clay 30B Nanocomposites at Different Clay Concentrations Without and with Ultrasonic Treatment

Samples (PA6/Cloisite® 30B/Amplitude)	Oxygen permeability (cm^3 mm/m^2/24 h)
Pure PA6	35.96
PA6/0%/0 μm	23.05
PA6/2.5%/0 μm	7.45
PA6/5%/0 μm	5.16
PA6/10%/0 μm	1.01
PA6/5%/5 μm	10.38
PA6/5%/7.5 μm	11.29
PA6/5%/10 μm	12.37

studied for use in food packaging applications. In particular, PA6/clay nanocomposites are a class of reinforced plastics, suitable for manufacturing packaging films, because of their nanodispersion structure when compared with conventional composites. Polymer-clay nanocomposites have an ordered nanolayer structure which provides the hurdles to oxygen entrance, where as conventional composites have voids for oxygen entrance in their microstructure. Oxygen permeability test of PA 6/clay nanocomposites were conducted to measure the effect of clay alone (Fig. 10). In addition, the combined effect of clay concentration and ultrasonic amplitude are summarized in Table III. From Figure 10, it is found that there is a significant continuous reduction of the oxygen permeability of nanocomposites with an increase in clay concentration. This is due to complete exfoliation of the clay during compounding process using the single screw mixing extruder. Again at a clay concentration of 10 wt % in the nanocomposites, the oxygen permeability was reduced by more than 20 times in comparison with the pure PA6. It is also found that oxygen permeability of nanocomposites increased with increasing ultrasonic amplitude (Table III). Hence, it is concluded that the permeability of nanocomposites decreased tremendously with increase of clay concentration. However, the permeability of nanocomposites is increased with ultrasonic treatment. The latter is possibly due to the presence of microvoids in films obtained from the PA 6/clay nanocomposites treated by ultrasound. This was indicated by change in the texture seen in the TEM micrographs of the untreated and ultrasonically treated nanocomposites (Fig. 7).

CONCLUSIONS

The significant dispersion of PA6/clay 30B nanocomposites was obtained without any chemical modification of the polymer matrix. Accordingly, a continuous ultrasonic extrusion method was developed to achieve a rapid intercalation and complete exfoliation of PA6/clay nanocomposites at all clay concentrations. Mechanical and rheological properties were affected by the ultrasonic treatment of PA6/clay nanocomposites. The structural properties of the PA6 were changed by the addition of clay and by ultrasonic treatment, which is supported by XRD and ^{15}NNMR studies of nanocomposites. The most significant effect is that the oxygen permeability of nanocomposites is tremendously decreased with increasing clay concentration.

The authors are grateful to the DST of Government of India for awarding BOYSCAST fellowship to S. K. Swain for this research at The University of Akron.

References

1. Ogawa, M.; Kuroda, K. Bull Chem Soc Jpn 1997, 70, 2593.
2. Okada, A.; Usuki, A. Mater Sci Eng 1995, 3, 109.
3. Giannelis, E. P. Adv Mater 1996, 8, 29.
4. Lebarion, P. C.; Wang, Z.; Pinnavaia, T. Appl Clay Sci 1999, 15, 11.
5. Gilman, G. W. Appl Clay Sci 1999, 15, 31.
6. Lan, T.; Pinnavaia, T. J Mater Res Soc Proc 1996, 79.
7. Oliver, W. C.; Pharr, G. M. J Mater Res 1992, 7, 1564.
8. Swallowe, B. J.; Sihna, S. K. Mechanical Properties and Testing of Polymers; Kluwer Academic Publishers: Dordrecht, 1999; p 113.
9. Schmidt, H. J Non Cryst Solids 1985, 73, 681.
10. Novak, B. M. Adv Mater 1993, 5, 422.
11. Mark, J. E. Polym Eng Sci 1996, 36, 2905.
12. Lorenzo, V.; Perena, J. M.; Faton, T. G. J Mater Sci Lett 1989, 8, 1455.
13. Miyasaka, K.; Ishikawa, K. J. Polym Sci Polym Phys 1968, 6, 1317.
14. Kyotani, M.; Mitsuhasi, S. J Polym Sci Polym Phys 1972, 10, 1497.
15. Kyotani, M. J. Macromol Sci Phys 1975, 11, 509.
16. Murthy, N. S. Polym Commun 1991, 32, 301.
17. Brucato, V.; Crippa, G.; Piccarolo, S.; Titomanlio, G. J Polym Eng Sci 1991, 31, 1411.
18. Wu, T. M.; Liao, C. S. Macromol Chem Phys 2000, 201, 2820.
19. Murthy, N. S.; Szollosi, A. B.; Sibilia, J. P.; Krimm, S. J. J Polym Sci Polym Phys Ed 1985, 23, 2369.
20. Hiramatsu, N.; Hirakawa, S. Polym J 1982, 14, 165.
21. Usuki, A.; Kayasumi, M.; Kojima, Y.; Okada, A.; Kurauchhi, T.; Kamigaito, O. J Mater Res 1993, 8, 1174.
22. Usuki, A.; Kayasumi, M.; Kojima, Y.; Okada, A.; Kurauchhi, T.; Kamigaito, O. J Mater Res 1993, 8, 1179.
23. Vijaya, R. V. K.; Koltypin, Y.; Palchik, O.; Gedanken, A. J Appl Polym Sci 2002, 86, 160.
24. Xia, H.; Wang, Q. J Appl Polym Sci 2003, 87, 1811.
25. Isayev, A. I.; Hong, C. K.; Kim, K. Rubber Chem Technol 2003, 76, 923.
26. Isayev, A. I.; Wong, C. M.; Zeng, X. Adv Polym Technol 1990, 10, 31.
27. Swain, S. K.; Isayev, A. I. Polymer 2007, 48, 281.
28. Lapshin, S.; Swain, S. K.; Isayev, A. I. Polym Eng Sci 2008, 48, 1584.
29. Ryu, J. G.; Kim, H.; Lee, J. W. Polym Eng Sci 2004, 44, 1198.

30. Ryu, J.; Kim, H. L. J Macromol Res 2002, 10, 187.
31. Lee, E. C.; Mielewski, D. F.; Baird, R. Polym Eng Sci 2004, 44, 1773.
32. Lapshin, S.; Isayev, A. I. J Vinyl Additive Technol 2007, 13, 40.
33. Oh, J. S.; Isayev, A. I.; Rogunova, M. A. Polymer 2003, 44, 2337.
34. Stejskal, E. O.; Memory, J. D. High Resolution NMR in the Solid State, Fundamentals of CP/MAS; Oxford University Press: New York, 1994; p 57.
35. Tukachinsky, A.; Schworm, T.; Isayev, A. I. Rubber Chem Technol 1996, 69, 92.
36. Swain, S. K.; Isayev, A. I. Polym Mater Sci Eng 2007, 96, 51.
37. Campoy, I.; Gormer, M. A.; Marco, C. Polym 1998, 39, 6279.
38. Wu, Q.; Liu, X.; Bergland, L. A. Macromol Rapid Commun 2001, 22, 1438.
39. Yoon, K.; Polk, M. B.; Min, B. G.; Schiraldi, D. A. Polym Int 2004, 53, 2072.